QUARTERLY PROGRESS REPORT

March 31, 1962

RESEARCH ON PHYSICAL AND CHEMICAL PRINCIPLES AFFECTING HIGH TEMPERATURE MATERIALS FOR ROCKET NOZZLES

UNION CARBIDE RESEARCH INSTITUTE
Tarrytown, New York

PARMA RESEARCH CENTER
Cleveland, Ohio

Laboratories of Union Carbide Corporation

Prepared by: Robert Lowrie
Robert Lowrie

Project Director: Verner Schomaker
Verner Schomaker

Submitted by: R. H. Crist
R. H. Crist, Director
UC Research Institute

Group Leader: Richard Kebler
R. W. Kebler

Contract No. DA-30-069-ORD-2787
Under the Auspices of
Advanced Research Projects Agency
and
U. S. Army Ordnance Missile Command

QUARTERLY PROGRESS REPORT

March 31, 1962

RESEARCH ON PHYSICAL AND CHEMICAL PRINCIPLES AFFECTING HIGH TEMPERATURE MATERIALS FOR ROCKET NOZZLES

UNION CARBIDE RESEARCH INSTITUTE
Tarrytown, New York

PARMA RESEARCH CENTER
Cleveland, Ohio

Laboratories of Union Carbide Corporation

Prepared by: Robert Lowrie
Robert Lowrie

Project Director: Verner Schomaker
Verner Schomaker

Submitted by: R. H. Crist
R. H. Crist, Director
UC Research Institute

Group Leader: Richard Kebler
R. W. Kebler

Contract No. DA-30-069-ORD-2787
Under the Auspices of
Advanced Research Projects Agency
and
U. S. Army Ordnance Missile Command

FOREWORD

This research program is being carried out in the research laboratories of Union Carbide Corporation located at Tarrytown, New York (Union Carbide Research Institute) and at Parma, Ohio (Parma Research Center). The work is supported by the Advanced Research Projects Agency under Contract No. DA-30-069-ORD-2787 with the U. S. Army Ordnance Missile Command, Redstone Arsenal, Alabama. The report period is from January 1, 1962 to March 31, 1962.

The program at Union Carbide Research Institute is under the project direction of Dr. Verner Schomaker with Dr. R. H. Crist serving as general project coordinator and Director of the Institute. Work at the Parma Research Center is under the supervision of Dr. R. G. Breckenridge.

The scope of the program as stated in the contract is "to obtain a better understanding of the mechanisms which govern the behavior of materials in high temperature environments, to learn how to make the most effective use of available materials, and to obtain a better knowledge of optimum properties desired for new materials for particular uses. The work is expected to provide guidance for those concerned with the development of materials and the use of materials in solid-propellant engines."

TABLE OF CONTENTS

I SUMMARY

Preliminary studies of the reactions of several new materials (HfB_2, HfC, and solid solutions of TiC/ZrC and ZrC/CbC) with possible rocket exhaust components such as CO_2, H_2O, HCl, and BF_3 have been made. Of the new compounds and solid solutions tested only HfC in oxidizing atmospheres appears to have attractive properties. Preliminary kinetic studies were conducted with TiC and ZTA graphite in mixtures of CO_2-CO-A. The corrosion of both materials depends linearly upon the partial pressure of CO_2 under the conditions of our experiment. The graphite was also shown to corrode nearly linearly with time. Metallographic studies have begun of carbide and boride samples that had been corroded in tests. New phases have been observed in several cases, and these will be further investigated. Studies of reactions between gases and refractory materials will be extended from the present 2200-2500°C to higher temperatures with emphasis on obtaining many results rapidly to survey the field.

The vaporization of ZrB_2 is being studied with a mass spectrometer. In addition to measuring the vapor pressures of boron and zirconium over ZrB_2, we have determined the vapor pressure, and from it the free energy and heat of vaporization, of zirconium as a function of temperature. These data are needed to calculate the heat of formation of ZrB_2, for which our results thus far indicate a value near -45 kcal/mole. Additional experiments will be performed on ZrB_2 in crucibles of different materials to verify our data. Equipment assembled during this quarter will be used to study both equilibrium and kinetic gas-solid reactions in the mass spectrometer.

The possibility that grain-boundary sliding produces the elastic damping found for polycrystalline tungsten between 600° and 1280°C was investigated. Specimens of various grain sizes and a monocrystalline sample were tested, and all showed similar behavior. Accordingly, grain boundary sliding is apparently not an important elastic-loss mechanism for tungsten at these temperatures. Similarly, the oscillation of dislocations does not appear to be the important mechanism, because recrystallizing a strain-hardened sample did not alter its anelastic behavior. Stress-induced ordering of interstitial atoms and solid-state reactions remain as recognized possible causes of the observed damping.

Precise measurements of the shear-wave attenuation and of the temperature dependence of the elastic constants of single-crystal tungsten will be undertaken during the next quarter. Two single crystals of TiC are now

being annealed and machined. Measurements of their elastic properties at elevated temperatures will also begin.

Data on the thermal expansion of zirconium carbide have been obtained up to 1770°C using a new x-ray furnace assembly. During this quarter it was found that the temperature measurements previously reported, made by sighting an optical pyrometer into a black-body hole, were in error. The large angular aperture of the micropyrometer was not being filled by radiation. This was a result of the size and alignment of the viewing holes through the furnace wall and radiation shields. This difficulty was corrected in the new furnace assembly, and the work on titanium carbide and tungsten was repeated using it. The data obtained on TiC, ZrC, and tungsten are in good agreement with the x-ray data of Mauer and Bolz over the entire temperature range within which they made measurements. Our data continue 425°C above their highest temperature, and we plan to extend this range upward by approximately 250°C during the next quarter.

Tensile creep tests were run on a tantalum specimen in the range 1025-1218°C to check operation of the creep equipment. A study was made of the compatibility of TiB_2 with tungsten, tantalum, and molybdenum to above 2100°C. Tantalum and tungsten did not react seriously with TiB_2 up to 2100°C, but molybdenum did. Grips of tantalum were used in testing two specimens of a commercial titanium diboride. The first test showed a creep rate of less than 1×10^{-4}/hr under a stress of 4,700 psi at 1515°C but was then spoiled by a power failure to the building, which caused overloading and fracture of the sample. During the second test the specimen overheated, reacted with the grips, and partially melted, apparently because of a thermocouple failure. Two remaining specimens of titanium diboride will be tested in creep above 1900°C during the next quarter. A calibration system for obtaining true specimen temperatures from the measured brightness temperatures will also be set up. A program on the mechanical properties of very pure tungsten in the range 1000-2500°C is being started. Special equipment will be designed and constructed to obtain and maintain very high purity in the tungsten tested.

The electrical resistivities and Hall coefficients of hot-pressed TiC, ZrC, HfC, CbC, and TaC have been measured over the range 4-300°K. These data have been interpreted in terms of a two-band model that can account for the properties measured and for the differences observed between the carbides of the IVa and Va Group metals. Work on solid solutions of IVa and Va carbides

is planned to explore further the curve of density of valence-electron states vs energy, with ZrC-CbC solutions to be studied first. An investigation of the effect of nitrogen additions on the galvanomagnetic properties of the refractory carbides is also planned. A furnace in which galvanomagnetic measurements can be made up to 1000°C will be constructed from a now-completed design.

The role of vacuum purification of refractory carbides and borides is becoming clearer. The metallic elements are seldom a problem, and most of them can be removed by a high-temperature vacuum treatment. Carbon, oxygen, and nitrogen pose the major difficulties. Nitrogen has been removed by vacuum treatments near 2250°C from TiC, TiB_2, and ZrB_2, but not from ZrC, for which higher temperature treatments will be tried. Oxygen and carbon contents appear to be related, as one would expect. These carbides and borides have generally contained more carbon (free carbon in carbides) than oxygen. Under these conditions oxygen has been relatively easy to remove, presumably as CO, at temperatures as low as 1500°C. However, the excess free carbon has been very difficult to remove when present in large amounts. Variations in procedure to more nearly balance the carbon and oxygen contents before vacuum treatment will be tried during the next quarter.

Continuing efforts have been made to produce specimens large enough for measurements of thermal conductivity (2" x 0.2" x 0.1"). A specimen of TiB_2 has been made, and others of TaC and CbC are nearly ready.

II INTRODUCTION

This program is concerned with the principles governing high-temperature chemical and physical behavior, especially in the respects that may contribute importantly to the successful performance of materials as rocket components operating at high temperatures.

The major group of materials being studied here consists of the refractory carbides and borides of the transition metals. The technology of these materials is not well advanced, a neglect due largely to their brittleness at room temperature. Consequently a considerable effort is being devoted to the preparation of powders of these compounds with good purity and to their fabrication into test specimens without contamination.

Corrosion and vaporization of a rocket nozzle material can importantly affect its practical performance. Direct loss of material and strength may be important, and the effects will be magnified if the attack is selective so as to produce cracks or accelerate their growth. It is for these reasons that gas-solid reactions and vaporization are being studied in this program. In particular, the program of chemical screening tests has been pursued during this reporting period to give a general view of the relative resistance of refractory carbides and borides to important component gases of rocket exhausts and to mixtures of these.

As structural parts, rocket nozzles are subjected to substantial stresses during operation. Some of these stresses change relatively slowly with time, and their effects on the nozzle will be determined by creep strength and ductility. There are also rapidly changing stresses, resulting from sudden heating or cooling. The resistance of the nozzle to such thermal shock will depend upon a combination of properties which it is enlightening to consider individually. The thermal stresses developed by a given temperature change increase with an increasing coefficient of expansion or elastic modulus, and they decrease with increasing thermal conductivity or specific heat. The ability to avoid fracture from these stresses depends upon the tensile strength and the ductility of the material. All these properties are being investigated for these reasons and some of them for others as well. Thus, a knowledge of the elastic modulus of his material is basic for any designer, and thermal conductivity and specific heat are necessary for calculations of heat transfer. In addition, a program of galvanomagnetic measurements at low temperatures is

being carried out to increase our knowledge of the behavior of electrons in these carbides and borides, and thus of the interatomic binding which is so important in determining their properties.

III TECHNICAL RESULTS AND PLANS

A. Gas-Solid Reaction Studies — I. R. Ladd, J. R. McDowell, and P. N. Walsh

1. Chemical Screening Tests

The exploratory investigation of the chemical reactivity of solid materials at high temperatures with various corrosive species, known or expected as combustion products from current or proposed rocket fuels, has been continued. The primary aim is to obtain qualitative information on the relative chemical stability of actual or prospective rocket-nozzle materials rather than detailed information of immediate applicability to rocket engineering. The nature and extent of the chemical reactions taking place, the mechanism of attack (i.e., grain boundary penetration, surface attack, etc.), the effects of sample purity, composition, and density, the dependance on gas composition, and the overall course of the reactions are all being considered. It is hoped that general patterns of behavior will be revealed that will be useful for predicting the relative chemical stabilities of the refractory materials in actual rocket applications.

The arc-image furnace has been used, in the manner described in the previous Semiannual Progress Report, for the measurement of the chemical reactivity of refractory carbides and borides and of graphite with the gases CO, CO_2, H_2, H_2O, HCl, and BF_3. In Table A-I are shown the experimental conditions (columns 1-5) and the corrosion results (columns 6 and 7). The rate of weight change is given per unit of surface area in column 6, since not all samples were the same size. These weight losses are re-expressed in column 7 as linear "corrosion rates" by dividing by the density (and multiplying by a mils/cm conversion factor). Although this corrosion rate must not be taken literally (the assumptions of constant sample density and uniform surface recession rate are often false), column 7 should be useful for indicating the linear corrosion rates of materials of widely differing densities.

A summary of "corrosion" rates of materials tested to date is included in Table A-II in order to facilitate comparison of the present data with that reported in the previous Semiannual Report. Comparisons should be made with caution for the following reasons:

a. The temperatures reported above 2400°C in the early runs are questionable even as brightness temperatures;

b. Temperature comparison between different materials is uncertain because the emittance factor may be different for every sample;

c. Gas pressure and flow rates were not the same for all runs;

d. The hot-pressed samples ranged in density from about 65% to 95% of theoretical (unless proven otherwise, reaction rate must be expected to depend strongly and unpredictably upon degree of compaction);

e. Until corrosion rates are proved to be linear with time, fine comparisons cannot be made between reactions terminated after different time intervals.

Metallographic examination of samples of corroded carbides and borides has been started in order to investigate the mechanism of attack and to identify the solid reaction products formed. Samples of TaC and TiB_2 that had previously been allowed to react with CO, CO_2, CO/H_2O, H_2, HCl, or BF_3 were sectioned, polished, and examined under a microscope.

TaC and TiB_2 samples that had been exposed to CO, H_2, HCl, or BF_3 showed no visible layer of reaction products in the polished section, though a thin surface layer could have been overlooked because the edges of the section were rounded in polishing. In contrast, layers of reaction products were plainly visible in the polished sections of TaC that had reacted with H_2O or CO_2. The exposure to a CO/H_2O mixture produced a layer 0.15-0.25 mm thick of a material with a Knoop hardness of 2500 (100g load) compared to 1500 for the unreacted TaC. This outer layer was much more readily attacked by an $HF-HNO_3$ electrolytic etch than was the remaining TaC. The TaC sample exposed to CO_2 lost its shape, and became covered with a lustrous, black coating. In the polished section two layers were revealed, an outer black layer (0.5-1.0 mm) and an inner light-yellow layer (0.3-0.6 mm) that resembled the layer on the TaC-in-CO/H_2O sample described above.

Reaction products with CO_2 and H_2O likewise were visible on the polished TiB_2 slices. In both cases the samples after reaction were distorted; the edges of the polished faces were no longer at right angles to each other. Attack by CO_2 produced a soft dark layer, 0.05 to 0.3 mm thick, covering the TiB_2 surface. Attack by CO/H_2O produced an unexplained phenomenon. Besides a very thin, dark layer coating the sample, a further new phase was found mingled with the TiB_2 to a depth of 1 mm. This new phase appeared almost entirely on opposite corners of the polished surface, one on an edge of the hot front face and the other on an edge of the cooler back face. No satisfactory explanation has been advanced for the unusual distribution.

Table A-I

Reaction	Time (min.)	Temp.[1] (°C)	Press[2] (mm)	Density[3] (g/cm^3)	Wt. Change Rate[4] x 10^4 ($gc/cm^2/min$)	Corrosion[5] Rate x 10^4 (mils/sec.)	Comments[6]
TiB_2 + CO/CO_2	4.5	2280	606-622	4.1	- 6.3	10	CO/CO_2 = 100
TiB_2 + H_2/H_2O[7]	3.5	2310	234-226	4.0	- 25	41	Black, porous surface
ZrB_2 + H_2/H_2O	3.5	2300	246-270	5.6	+ 3.0	- 7	Thin white coating
HfB_2 + CO	4.5	2260	604-614	7.3	- 0.94	0.8	
HfB_2 + CO_2	2.5	2250	600-646	7.9	- 130	120	Heavily reacted; misshapen
HfB_2 + HCl	4.5	2200	588-662	8.2	- 360	290	Crumbly surface
TiC + CO_2	1.5	2240	606-618	4.2	- 870	1350	Melted surface; P_{CO_2} = 606 mm
TiC + CO/CO_2	4.5	2270	606-636	4.3	- 3.9	6	CO/CO_2 = 100; P_{CO_2} = 6 mm
TiC + CO/CO_2	4.5	2270	598-646	4.3	- 13.3	20	CO/CO_2 = 25; P_{CO_2} = 23 mm
TiC + CO/CO_2	4.5	2260	605-606	4.2	- 15.3	24	CO/CO_2 = 10; P_{CO_2} = 55 mm
TiC + CO/CO_2	5.5	2270	604-620	4.1	- 190	300	CO/CO_2 = ½; P_{CO_2} = 151 mm
TiC + CO/CO_2	5.5	2240	604-624	4.2	- 450	710	CO/CO_2 = 1; P_{CO_2} = 302 mm
TiC + CO/CO_2	1.5	2250	604-620	4.2	- 690	1100	CO/CO_2 = 0.33; P_{CO_2} = 453 mm
ZrC + H_2/H_2O	3.5	2250	240-236	5.8	+ 27	- 50	Thin white coating
HfC + CO_2	3.2	2340	602-632	9.2	+ 85	- 64	White coating; melted spot
HfC + CO/CO_2	4.5	2290	604-618	9.1	+ 0.46	- 0.3	CO/CO_2 = 100
HfC + H_2/H_2O	3.5	2250	240-236	8.4	+ 12	- 10	Thin, grayish coating
HfC + H_2	4.5	2250	636-652	9.0	- 9.0	7	
HfC + HCl	4.5	2280	616-734	9.0	- 200	150	Thin, cream-colored coating
HfC + BF_3	4.5	2250	636-650	9.2	- 190	130	Black surface

TABLE A-I - Continued

Reaction	Time (min.)	Temp.[1] (°C)	Press[2] (mm)	Density[3] (g/cm^3)	Wt. Change Rate[4] x 10^4 ($gc/cm^2/min$)	Corrosion[5] Rate x 10^4 (mils/sec.)	Comments[6]
CbC + CO/CO_2	4.5	2310	606-608	7.0	- 17	9	CO/CO_2 = 100; Gold surface
CbC + H_2/H_2O	5.5	2280	238-240	7.0	+ 9.5	- 9	Black, melted surface
CbC + HCl	4.0	2210	602-668	7.2	- 59	54	Thin gold-blue coating
Ta_2C + CO_2	2.5	2250	604-640	10.4	(-1/3)	-	Lustrous black coating; welded to holder
Ta_2C + HCl	4.5	2280	600-632	10.4	-180	110	Yellow surface
TiC/ZrC + CO_2	5.0	2290	600-608	4.4	Unweighable	-	Porous, misshapen surface
TiC/ZrC + CO/CO_2	4.5	2380	608-624	4.4	+ 1.3	- 2	CO/CO_2 = 100
TiC/ZrC + H_2/H_2O	5.5	2300	244-246	4.3	+ 29	- 45	Gray, crumbly surface
TiC/ZrC + HCl	4.5	2250	610-650	4.7	- 96	140	Yellow surface
TiC/ZrC + HF_3	4.5	2260	620-640	4.4	- 44	65	Black surface
ZrC/CbC + CO_2	2.0	2240	620-616	5.9	+120	- 93	Gray, melted droplets
ZrC/CbC + HCl	2.1	2220	612-626	6.2	- 80	[illegible]	Gray surface
ZTA Graphite + A/CO_2	5.0	2250	650-680	1.9	- 91	515	A/CO_2 = 3.33 Sample distorted

NOTES:
1. These are brightness temperatures. During a run variations of 50°C were frequently observed.
2. Initial and final pressure readings, listed in that sequence.
3. The bulk density of each solid piece was calculated from weight and dimension measurements.
4. Weight change rate = grams change (gain or loss)/cm^2/min.
5. "Corrosion rate" = $\frac{\text{weight change (g)} \times 394 \text{ mil/cm}}{\text{bulk density } (g/cm^3) \times \text{area } (cm^2) \times \text{time (sec.)}}$
6. Comments pertain to appearance of solid samples after reaction.
7. All H_2/H_2O mixtures were prepared by bubbling H_2 through distilled water at room temperatures.

TABLE A-II SUMMARY OF "CORROSION RATES"

	CO		CO_2		CO/CO_2=100		CO/H_2O		H_2/H_2O		H_2		HCl		BF_3	
Compd.	Temp[1] (°C)	Corr Rate[2]	Temp (°C)	Corr Rate	Temp (°C)	Corr Rate	Temp (°C)	Corr Rate	Temp (°C)	Corr Rate	Temp (°C)	Corr Rate	Temp (°C)	Corr Rate	Temp (°C)	Corr Rate
TiB_2	2050	-1.0[3]	2030	620	2280	10	2290	240	2310	41	2170	0.4	2100	37	2200	160
ZrB_2	2400	-8.8	2600	-39			2700	-46	2300	-7	2430	6.1	2000	200	2350	260
HfB_2	2260	0.8	2250	120									2200	290		
CbB_2	2370	1.8	2200	-46			2260	-4.0	2200	49	2220	-1.2	2280	35	2260	56
TaB_2	2300	3.7	2240	(1/3)[4]			2240	2.4	2230	-6.8	2250	1.9	2230	60	2240	33
TiC	2700	3.9	2240	1350	2270	6	2240	320	2230	155	2470	3.7	2450	27	2350	57
ZrC	2700	2.0	2500	-120			2460	30	2250	-30	2300	2.5	2100	38	2500	48
HfC			2340	-64	2290	-0.3			2250	-10	2250	7	2280	150	2250	130
CbC	2700	0.16	2700	(1/2)	2310	9	2250	(1/3)	2280	-9	2500	3.2	2210	54	2050	6.2
TaC	2300	0.81	2250	(1/3)			2250	180	2230	8.4	2100	-.4	2200	30	2190	29
Ta_2C			2250	(1/3)									2280	110		
TiC/ZrC			2290	(1/4)	2380	-2			2300	-45			2250	140	2260	65
ZrC/CbC			2240	-93									2220	85		
ATJ	2360	1.6	2300	940			2280	210	2240	190	2330	21	2200	18	2130	1.0
ZTA	2420	2.3	2360	730			2270	180	2230	93	2370	14	2200	9.7	2320	10
W	2220	0.9	2220	74	2270	0.2	2240	15	2220	0.38	2240	0.37	2230	4.2	2240	15

NOTES:

1. These are brightness temperatures.
2. "Corrosion rate", as defined in Table A-I, Note 5, in mils/sec x 10^4.
3. A negative corrosion rate means increase in sample weight, usually by buildup of a coating.
4. Fractions represent the estimated volume of sample removed by reaction.

TABLE A-III Effect of CO_2 Pressure on Corrosion of ZTA Graphite and TiC

Reaction	Time (min)	Temp[1] (°C)	Orig. Wt. (g)	Wt. Loss (g)	Gas Partial Pressure (mm) CO_2	A	CO	Initial Surface Area (cm^2)	Initial Volume (cm^3)	Density (g/cm^3)	Corrosion[2] Rate x 10^4 (mils/sec)
ZTA + A/CO_2											
Run 1	4.5	2300	0.2340	0.0013	6	642		1.59	0.124	1.89	6
Run 6	4.5	2280	0.2514	0.0210	60	590		1.62	0.129	1.94	100
Run 11	4.5	2260	0.2408	0.0677	150	500		1.55	0.122	1.97	320
Run 9	4.0	2260	0.2320	0.0876	250	400		1.55	0.122	1.90	490
Run 12	3.0	2250	0.2373	0.0944	350	300		1.55	0.122	1.94	690
Run 10	2.5	2280	0.2330	0.0990	450	200		1.55	0.122	1.91	880
TiC + CO/CO_2											
Run 1	4.5	2270	0.5125	0.0027	6		600	1.53	0.119	4.29	6
Run 8	4.5	2270	0.4386	0.0093	23		575	1.39	0.103	4.26	20
Run 2	4.5	2260	0.5853	0.0118	55		550	1.71	0.138	4.24	24
Run 5	3.5	2270	0.3910	0.0845	151		473	1.32	0.096	4.07	295
Run 3	3.5	2240	0.4506	0.2258	302		302	1.44	0.108	4.16	710
Run 7	1.5	2250	0.4443	0.1467	453		151	1.42	0.106	4.16	1090
Run 4	1.5	2240	0.4614	0.1917	606		-	1.43	0.109	4.25	1350

NOTES:

1. Brightness temperatures.
2. "Corrosion rate" = $\frac{\text{wt. lost(g)} \times 394 \text{ mil/cm}}{\text{density } (g/cm^3) \times \text{area } (cm^2) \times \text{time (sec)}}$

TABLE A-IV Effect of Time on Corrosion of ZTA Graphite by A/CO_2

Run No.	Time (min)	Temp[1] (°C)	Orig. Wt. (g)	Wt. Loss (g)	Partial Press (mm) CO_2	Partial Press (mm) A	Initial Area (cm^2)	Initial Volume (cm^3)	Density (g/cm^3)	Corrosion[2] (mils)	Wt. Loss Rate x 10^4 ($g/cm^2/min$)
20	1.0	2250	0.2511	0.0174	150	500	1.62	0.129	1.95	2.16	110
22	1.5	2250	0.2442	0.0199	150	500	1.61	0.128	1.91	2.56	83
24	1.5	2250	0.2424	0.0275	150	500	1.61	0.128	1.89	3.54	115
16	2.0	2250	0.2487	0.0355	150	500	1.61	0.128	1.94	4.49	110
25	2.5	2250	0.2477	0.0344	150	500	1.61	0.128	1.93	5.64	110
17	3.0	2250	0.2466	0.0499	150	500	1.61	0.128	1.93	6.35	105
26	3.5	2250	0.2450	0.0607	150	500	1.62	0.129	1.90	7.76	110
28	3.67	2250	0.2492	0.0597	150	500	1.61	0.128	1.94	7.49	100
18	4.0	2250	0.2462	0.0594	150	500	1.60	0.127	1.94	7.52	93
27	4.5	2250	0.2425	0.0702	150	500	1.61	0.128	1.89	9.06	97
19	5.0	2250	0.2432	0.0734	150	500	1.61	0.128	1.90	9.45	91
23	5.5	2250	0.2463	0.0802	150	500	1.61	0.128	1.93	10.80	93
30	6.25	2250	0.2465	0.0895	150	500	1.62	0.129	[illegible]	11.30	88
29	7.0	2250	0.2450	0.0970	150	500	1.62	0.129	1.90	12.42	86

NOTES:

1. Brightness temperature.
2. "Corrosion" = $\frac{\text{wt. loss (g)} \times 394 \text{ mil/cm}}{\text{density } (g/cm^3) \times \text{area } (cm^2)}$

TABLE A-V Development of Porosity During Reaction

Reaction	Time (min)	Temp[1] (°C)	Dimensional Decrease (mm) Measured	Dimensional Decrease (mm) Calculated[2]	Calculated Density (g/cm^3) Initial	Calculated Density (g/cm^3) Final
HfC + HCl	4.5	2280	.03 x .06 x .09	0.200	8.98	8.14
CbC + HCl	4.0	2210	.03 x .04 x .04	0.066	7.18	7.05
Ta_2C + HCl	4.5	2280	.02 x .06 x .04	0.155	10.40	9.52
TiC/ZrC + HCl	4.5	2250	.05 x .04 x .08	0.184	4.69	4.25
TiC/ZrC + BF_3	4.5	2260	.00 x .02 x .03	0.089	4.45	4.21
ZrC/CbC + HCl	2.1	2220	.01 x .03 x .05	0.053	6.22	6.14
ZTA + A/CO/CO_2						
Run 1	4.5	2300	.01 x .01 x .01	0.009	1.89	1.89
Run 2	4.5	2290	.005 x .005 x .00	0.023	1.89	1.86
Run 3	4.5	2280	no change	0.015	1.89	1.87
Run 4	4.5	2280	.01 x .01 x .00	0.023	1.88	1.86
Run 5	4.5	2300	no change	0.027	1.89	1.86
Run 6	4.5	2280	.02 x .02 x .02	0.140	1.94	1.80
Run 7	4.5	2300	.015 x .015 x .015	0.130	1.87	1.73
Run 8	4.5	2280	.03 x .02 x .04	0.157	1.92	1.76

NOTES:

1. Brightness temperatures.
2. Dimensional decrease = $\frac{2 \times \text{wt. decrease (g)} \times 10 \text{ mm/cm}}{\text{initial density } (g/cm^3) \times \text{initial area } (cm^2)}$

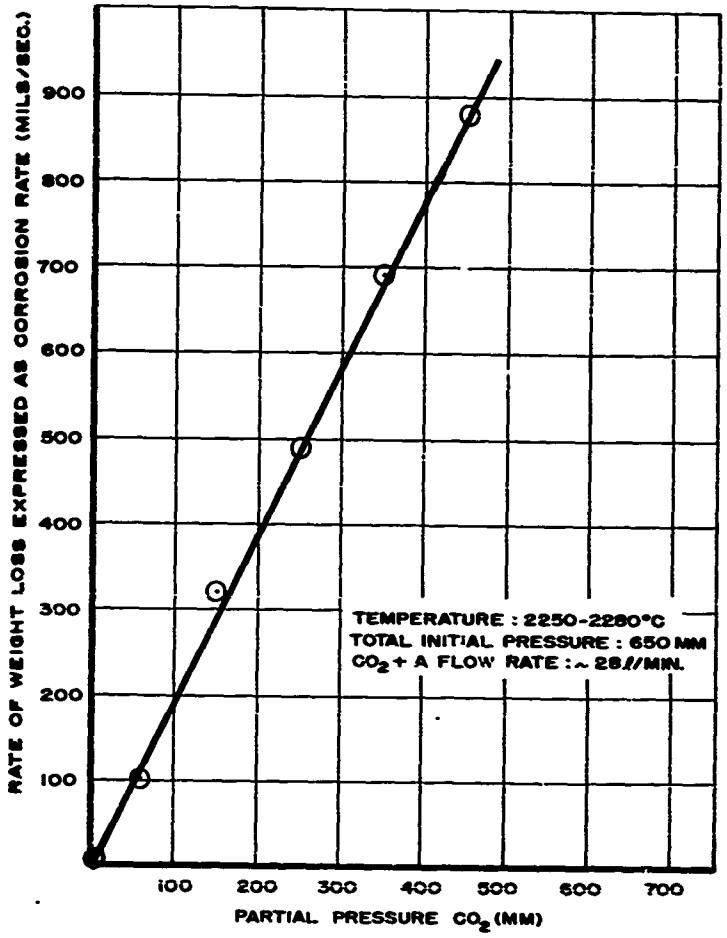

FIGURE A-1 CORROSION RATES OF ZTA GRAPHITE IN CO_2

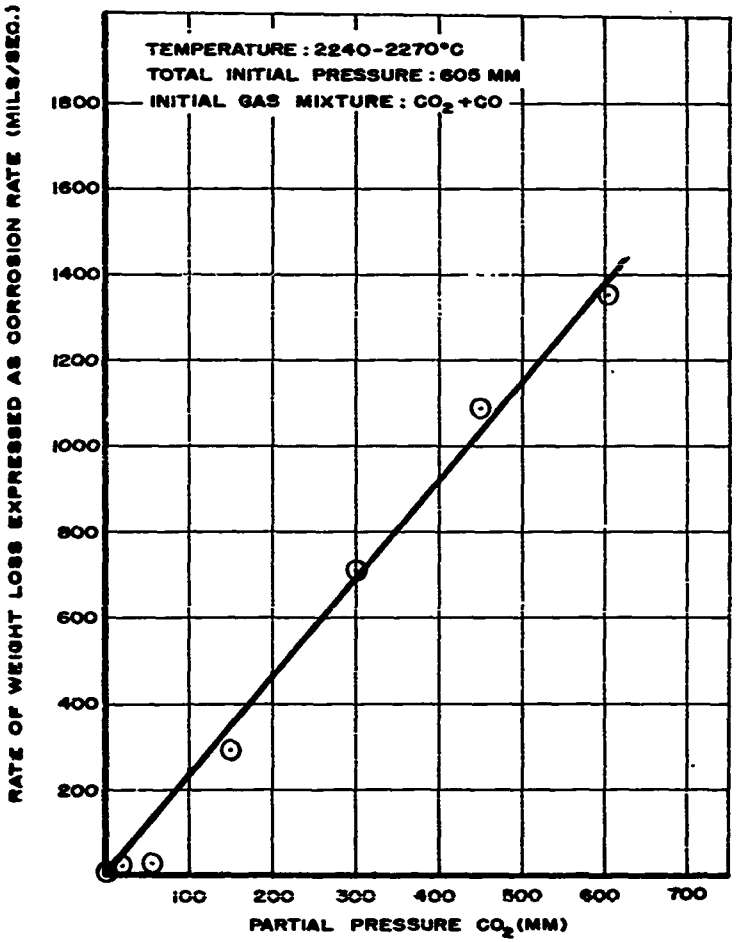

FIGURE A-2 CORROSION RATES OF TiC IN CO_2

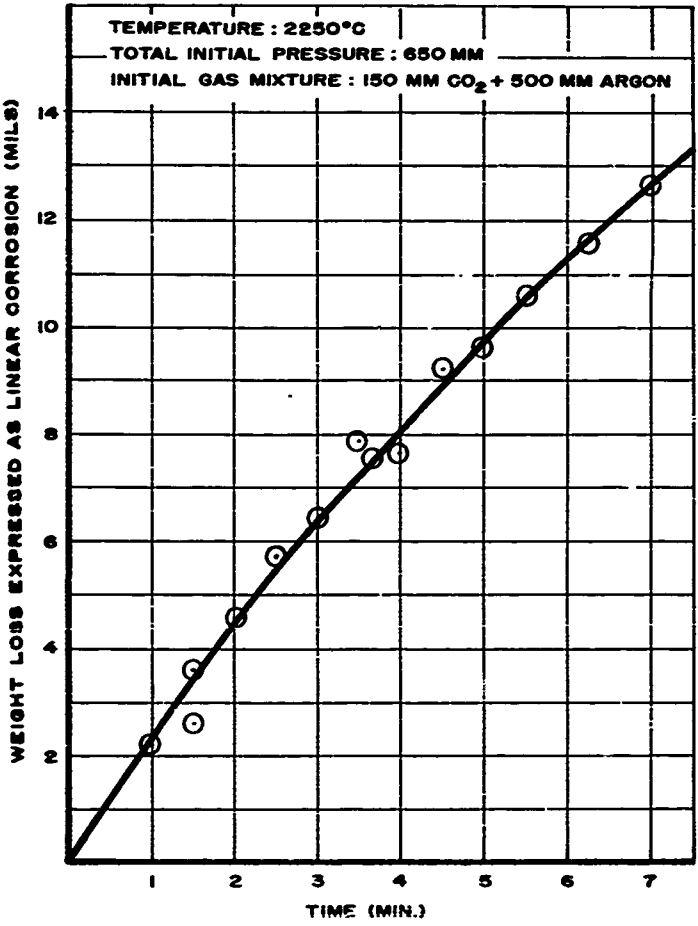

FIGURE A-3 LINEAR CORROSION OF ZTA GRAPHITE VS. TIME

2. Kinetic Studies

Some preliminary kinetic studies have been performed with TiC and ZTA graphite, primarily to test the capability of the arc-image-furnace equipment. Graphite was used because an adequate supply of material was readily available. The data collected from these studies are recorded in Tables A-III and A-IV. Figure A-1 shows a plot of corrosion rate of ZTA graphite (calculated from weight-loss data) vs. partial pressure of CO_2. The straight-line plot shows that the reaction rate is first order with respect to the partial pressure of CO_2 in the range 5-450 mm. Figure A-2 shows a similar plot of the calculated corrosion rate of TiC (83-88% dense) vs. partial pressure of CO_2.

The results of a study of the linear corrosion of ZTA graphite vs. time are shown in Figure A-3 and Table A-IV. From the changing slope of the curve it might appear that the fundamental reaction rate decreases with time. Since the linear corrosion was calculated by dividing the sample weight loss by the product of the sample density and original surface area, a correction should be made for the decrease in surface area that occurs during reaction. The issue is confused by the fact that the samples become more porous during corrosion, but it does seem that the specific reaction rate decreases somewhat with time. By the same token, a uniform rate of linear surface recession calculated from weight-loss measurements would not necessarily express the actual dimensional change of the sample. In a number of experiments where it has been possible to measure the dimensions of the sample after reaction the actual dimensional change has been found to be considerably less than that calculated, indicating increased porosity (decreased density) of the sample (Table A-V). These observations suggest that a substantial fraction of the observed reaction takes place within pores in the sample; it would seem that increasing the density of the initial sample would therefore reduce the amount of reaction observed. An experimental test of this variable will be made using arc-grown polycrystalline materials.

3. Future Work

The present experimental approaches and evaluation techniques will be applied to new materials as samples become available. These techniques will also be extended to higher temperatures with equipment now being set up. An increasing emphasis will be placed upon supplementary experiments designed to help interpret previous results and possibly relate them more directly to rocket operating conditions.

B. Thermodynamics and Kinetics of Vaporization

1. Mass-spectrometer Studies of Vaporization — O. C. Trulson, H. W. Goldstein

A substantial part of our mass-spectrometric work has been on the refractory borides, first on TiB_2 and now on ZrB_2. The TiB_2 study[1] served mainly to define the ΔH of formation, previously quite uncertain, at $\Delta H^\circ_{f\ 298}$ = -52 kcal/mole. An auxiliary result, important for the present study, was a confirmation of 132 kcal/mole as the heat of vaporization of boron.

For ZrB_2 the best published values of $\Delta H^\circ_{f\ 298}$ also disagree badly: -77 kcal/mole from a calorimetric determination by Huber, Head, and Holley,[2] and -57 kcal/mole from a vaporization study by Leitnaker, Bowman, and Gilles,[3] who, however, favored the -77 value. In their calculations they had used the Skinner, Edwards, and Johnston vapor-pressure data[4] and the JANAF[5] $-(F^\circ-H^\circ_{298})/T$ functions to obtain $\Delta H^\circ_{vap\ 298}$ = 145.5 kcal/mole for Zr, and this result, they suggested, was in error.

As reported last Quarter, boron and zirconium signals, corresponding to

$$ZrB_2(s) \rightleftharpoons Zr(g) + 2\,B(g) \quad , \tag{1}$$

were observed when ZrB_2 was heated in a tungsten-lined tantalum Knudsen cell, whereas with a graphite cell only boron signals, corresponding to

$$ZrB_2(s) + C(s) \rightleftharpoons ZrC(s) + 2\,B(g) \quad , \tag{2}$$

were found. The tungsten cell obviously reacted with the ZrB_2 at temperatures above 2400°K and there were ZrO as well as Zr and B signals, there were doubts about the propriety of assuming reaction (2), and the heat of vaporization of zirconium had in any case to be questioned, but the tentative results clearly favored the lower magnitude for the heat of formation of ZrB_2.

We have now made further measurements on ZrB_2 in graphite as well as

---

(1) Semiannual Progress Report, June 30, 1961, Contract DA 30-069-ORD-2787.

(2) E. J. Huber, E. L. Head, and C. E. Holley, Jr., unpublished work, cited in (3).

(3) J. M. Leitnaker, M. G. Bowman, and P. W. Gilles, J. Chem. Physics 36, 350 (1962).

(4) G. B. Skinner, J. W. Edwards, and H. L. Johnston, J. Amer. Chem. Soc., 73, 174 (1951).

(5) JANAF INTERIM THERMOCHEMICAL TABLES, The Dow Chemical Company, Midland, Michigan, December 31, 1960.

on Zr in ZrC-lined graphite and ZrB_2 in ZrC-lined graphite. Interpretation of the ZrB_2 work is as yet incomplete, so no details will be given here. The indications are that the heat of formation of ZrB_2 is even less than 57 kcal/mole. The Zr work, reported in some detail below, agrees fairly well with the Skinner, Edwards, and Johnston data, and so negates the argument of Leitnaker et al. against the lower result for the ZrB_2 heat of formation.

a. Zirconium and Zirconium Diboride in Zirconium Carbide. Since the reaction of zirconium diboride with carbon yielded only boron as a volatile species, it was concluded that a graphite crucible could not be used to study the vaporization of zirconium diboride. And, although Leitnaker, Bowman, and Gilles[3] used a tungsten crucible, our preliminary study showed that zirconium diboride and tungsten react to form a liquid phase at approximately 2450°C. As an alternative, a zirconium carbide crucible was chosen since the zirconium-boron-carbon phase diagram[6] indicates that zirconium diboride should be stable with zirconium carbide.

To prepare a zirconium carbide crucible, a graphite crucible was lined with zirconium, loaded with zirconium and zirconium diboride, and heated to approximately 1800°C for several hours. Visual inspection showed that the inside of the crucible had acquired a coating, which was identified as zirconium carbide by x-ray analysis. Additional zirconium was added to the crucible, as was a silver calibration sample;[7] then the heating cycle was repeated, and the vapor pressure of zirconium was determined below its melting point.[5] Additional zirconium was added with a second calibration charge, and the zirconium vapor pressure was determined both above and below the melting point. Since data taken below the melting point after the zirconium had once been melted agreed with the vapor pressure data obtained before melting, it seemed clear that the zirconium carbide coating on the inside of the crucible had become sufficiently thick to adequately limit the rate of formation of further zirconium carbide. It is therefore believed that the observed pressures represent the true vapor pressure of zirconium.

Table B-I presents the observed zirconium vapor pressure, together with the computed free energy ($\Delta F_T^\circ = -RT\ln P_{Zr}$) and the "third-law" standard

(6) H. Nowotny, E. Rudy, and F. Benesovsky, Mh. Chem., 92, 393 (1961).

(7) W. A. Chupka and M. G. Inghram, J. Phys. Chem., 59, 100 (1955).

enthalpy of vaporization obtained with the JANAF[5] $-(F^\circ - H^\circ_{298})/T$ functions, for each of the series of runs. The data were also plotted as log P_{Zr} vs. T^{-1} as shown in Figure B-1. The heat of sublimation value derived by least squares from the data above the melting point is 137.5 ± 5.9 kcal/mole, and from the data below the melting point is 142 ± 10 kcal/mole. These results are to be compared with the average third-law value, 140.9 ± 3.1 kcal/mole, and with the value 145.5 kcal/mole calculated from the vapor-pressure data of Skinner, Edwards, and Johnston.[4] The difference of approximately 4.5 kcal/mole does not account for the difference in the values of the heat of formation of zirconium diboride as determined by Leitnaker, Bowman, and Gilles[3] and by Huber, Head, and Holley.[2]

Boron-pressure data were taken in addition to the zirconium measurements at temperatures above the melting point of zirconium in the experiments just discussed. Preliminary examination of these results suggests that the heat of formation of zirconium diboride must be near 50 kcal/mole.

b. Plans. Additional experiments will be performed on ZrB_2 in zirconium carbide and on ZrB_2 in tungsten. Equipment has been fabricated to provide a gas inlet system for the mass spectrometer, and a molecular beam assembly under construction is nearly complete. This new equipment will be used both for equilibrium and kinetic gas-solid reaction studies.

Table B-I

Thermodynamic Data for Zirconium

Temp. (°K)	P_{Zr} (atm.)	ΔF°_{T} (kcal/mole)	$\Delta H^{\circ}_{vap\ 298}$ (kcal/mole)
2093	2.91×10^{-8}	72.16	141.07
2033	1.20×10^{-8}	73.69	140.69
2003	7.22×10^{-9}	74.63	141.77
1968	3.54×10^{-9}	76.11	141.06
2080	2.46×10^{-8}	72.42	140.90
2092	2.80×10^{-8}	72.30	141.16
2024	1.04×10^{-8}	73.94	140.65
1984	5.62×10^{-9}	74.90	140.35
2070	2.13×10^{-8}	72.67	140.83
2047	1.32×10^{-8}	73.80	141.24
2082	2.57×10^{-8}	72.31	140.85
2112	4.40×10^{-8}	71.09	140.57
2148	6.97×10^{-8}	70.35	140.97
2148	7.63×10^{-8}	69.96	140.58
2171	1.17×10^{-7}	68.87	140.21
2193	1.53×10^{-7}	68.55	140.74
2216	1.81×10^{-7}	68.37	141.13
2236	2.56×10^{-7}	67.45	140.83
2257	3.25×10^{-7}	67.01	141.05
2274	3.86×10^{-7}	66.73	141.31
2067	2.13×10^{-8}	72.57	140.64
2095	3.10×10^{-8}	71.99	140.94
2060	1.65×10^{-8}	73.37	141.12
2109	4.82×10^{-8}	70.61	140.00
2152	7.75×10^{-8}	70.03	140.77
2190	1.16×10^{-7}	69.51	141.45
2050	1.58×10^{-8}	73.73	141.26
2086	2.39×10^{-8}	72.76	141.43
2117	3.99×10^{-8}	71.68	141.32
			Avg: 140.9

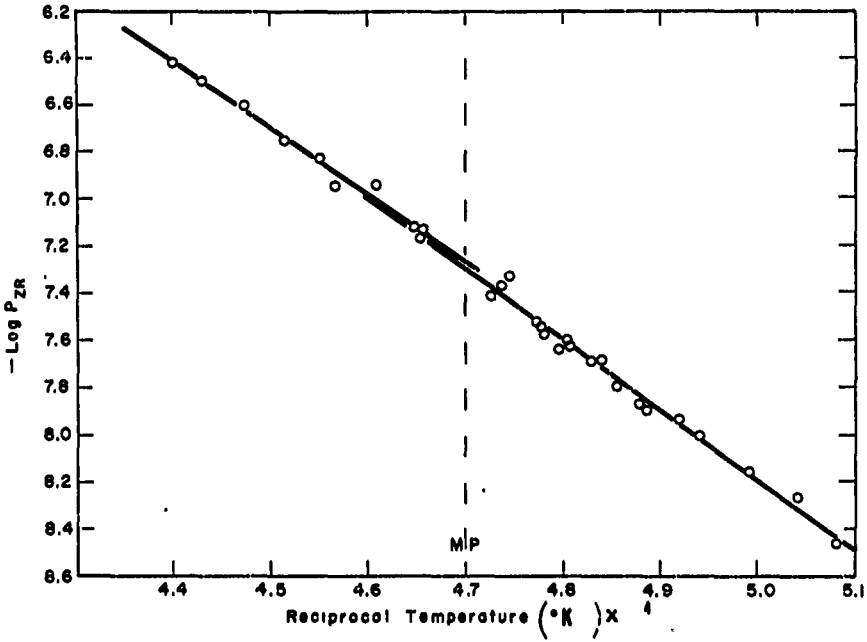

FIGURE B-1. LOG OF VAPOR PRESSURE OF ZIRCONIUM METAL VS RECIPROCAL TEMPERATURE.

2. Matrix Isolation Studies W. Weltner

This work was initiated in order to study the vibrational and electronic properties of the molecules which vaporize from high-temperature materials. Since it will be used in only a limited way in the future, a summary of the present position seems appropriate. A technique for freezing-out high-temperature molecules has been worked out, and it has been shown that individual molecules can be isolated in a solid inert gas at low temperatures (4°K or 20°K). This has been demonstrated quite conclusively by studies on the vapor evolving from boric oxide at 1400°K and from carbon at 2600°K.

In the case of B_2O_3, a study of the vibrational spectrum of the matrix isolate has led to a considerable change in the assignment of the vibrational fundamentals in the molecule, which has led in turn to changes in the calculated thermodynamic properties. The most noteworthy advantage of the low temperature study is the increased spectral resolution that was attained. B^{10} and B^{11} isotopic effects in the spectrum are clearly seen, which is not true in the high temperature studies of such species.

Carbon vapor has been trapped in solid inert gases, and the electronic spectrum of the matrix thus formed contains a band system near 4050 Å which corresponds to that of gaseous C_3. The complex C_3 spectrum, as it appears in hot carbon vapor, has been puzzling for many years, and a study of this spectrum at 4°K has several advantages. The possible vibrational and electronic transitions are now quite restricted, and (as noted above for B_2O_3) the spectral bands are narrowed; thus, analysis of the spectrum may be feasible.

If the temperature of the matrix is raised somewhat, so that the trapped carbon molecules can diffuse and react with each other, the spectrum changes greatly, no doubt because larger molecules (C_4, C_5, etc.) are formed. At present there is no other way to study these larger molecules since their concentration in the vapor, under normally attainable conditions, is quite small. This illustrates another general approach that can be applied to high-temperature molecules.

The main disadvantage is the perturbing effect which the matrix has upon the trapped molecules. However, this effect may often be small or otherwise subject to analysis and correction, and it will usually be outweighed by the many advantages of the matrix-isolation technique. A promising future is foreseen for matrix-isolation studies of high-temperature vapors.

C. Elastic Properties

B. T. Bernstein

The elastic properties of refractory materials have great practical usefulness for design calculations and important fundamental significance in the field of cohesive properties of solids. Since the dynamic elastic constants of a material may be calculated from the velocities of elastic shear and compressional waves in it, equipment for measuring these velocities by a modified pulse-echo technique has been built and is being used for making such measurements as a function of temperature. In addition, the signal will be attenuated as a result of any inelastic losses of the wave energy. Such losses may be caused by grain-boundary sliding, stress-induced ordering of interstitial atoms, alternate precipitation and dissolution of a new phase, or by other processes.

1. High-Temperature Vacuum Furnace

A new resistance-heated vacuum furnace has been assembled which has several new features. Tungsten replaces tantalum in the heater elements and radiation shields so that higher temperatures may be reached. Water-cooled split collars support the heater and shields more rigidly and make their replacement much easier. The heater is divided into three independently powered sections, instead of the two used previously, to give closer control of temperature gradients in the sample and to increase the operating temperature range. The furnace has been operated at 2000°C with a 2.5 KW power input. The vacuum was 5×10^{-7} Torr at this temperature and 3×10^{-7} Torr at room temperature after bakeout.

2. Polycrystalline Tungsten

Elastic measurements previously made[1-3] up to 1800°C on a polycrystalline sample of tungsten (W-1) had revealed the occurrence of appreciable elastic losses, starting in the range 600-800°C and increasing rapidly in the range 1220-1280°C until no shear-signal transmission could be detected. No difference was found in the attenuation for the sample in the cold worked

---

1. Semiannual Progress Report, June 30, 1961, Contract No. DA-30-069-ORD-2757.
2. Semiannual Progress Report, December 31, 1961.
3. B. T. Bernstein, to be published in J. Appl. Phys.

condition and after heating to 1800°C. Metallography now reveals that the microstructure of the sample had changed from the typical distorted fine-grained structure of cold-worked tungsten to one of coarse equiaxed grains (64 grains per sq mm). Since this large structural change did not affect the elastic losses, it appears that they are not caused by relative grain motion.

As a further check on this conclusion, a second sample (PW-2) obtained from a different manufacturer was annealed at 2200°C to produce an even coarser microstructure of 32 grains per sq. mm. The attenuation results obtained with PW-2 were closely similar to those of PW-1 up to 1070°C, where the measurements had to be discontinued to repair a faulty electrical connection in the furnace.

3. Single-Crystal Tungsten

As a final step in determining the influence of grain boundaries upon attenuation, experiments have begun at elevated temperatures with single crystals of tungsten. Crystal LW-2 contains some lineage structure, but the < 100 > axes of its subgrains lie within 2.3°-4.1° of the cylindrical sample axis, parallel to which the sonic wave travels. According to preliminary results, LW-2 is similar to the polycrystalline samples in the temperature dependence of the attenuation of 10 MC/sec shear waves. Preliminary measurements have also been obtained for the velocity and attenuation of compressional waves in LW-2 up to 1400°C. There is no previous report of dynamic elastic-property measurements on metal single crystals at temperatures as high as 1400°C.

4. Qualitative Interpretation of Results

As discussed in previous reports,[1,2] the four factors which seem most likely to cause the shear-wave attenuation effects observed in tungsten are: (1) relative motion of the grains of a polycrystalline material at elevated temperatures, (2) stress-induced ordering of interstitial impurity atoms into preferred sites in the body-centered-cubic tungsten lattice, (3) oscillation of dislocations under the influence of an applied stress, and (4) solid state reactions, such as precipitation.

Relaxation effects due to the relative motion of the grains of a polycrystalline solid at elevated temperatures should be a function of the

size and distribution of grains.[4] The results obtained on samples FW-1 and FW-2 show that heat treatment and grain size do not affect the magnitude of the elastic-loss or its temperature dependance. Likewise, the observed similarity of measurements on single crystal LW-2 to the results obtained on samples FW-1 and FW-2 indicates that grain boundary relaxation is not the cause of the elastic loss.

Dislocations formed by plastic flow in the course of the machining of the samples do not seem to be an important factor, since extensive annealing of sample FW-2 did not affect the magnitude or temperature dependance of the signal amplitude. This is contrary to what would be expected if the oscillation of dislocations under an applied stress[5] were the mechanism of the observed damping. On the basis of the results obtained to date on both polycrystalline and monocrystalline samples of tungsten, it is felt that the mechanisms most probably responsible for the observed shear-wave damping effects are stress-induced ordering of interstitial atoms or solid-state reactions.

5. Future Work

Precise measurements of shear-wave attenuation and of the temperature dependance of the single-crystal elastic constants of tungsten will be undertaken. Two single crystals of TiC, for which room temperature measurements have been reported,[2] will be annealed and then machined, and measurements of their elastic properties at elevated temperatures will be started.

---

4. C. Zener. Elasticity and Anelasticity of Metals, University of Chicago Press, Chicago, Illinois. 1948.

5. D. H Niblett and J. Wilks. Phil. Mag. Suppl. 9, 68 (1960).

D. X-Ray Studies

C. R. Houska

X-ray diffraction experiments at elevated temperatures are being used to determine both the thermal expansion of materials and the mean vibration amplitudes of the atoms which compose them. Results obtained for the thermal expansion and atomic vibration amplitudes of tungsten and titanium carbide have been included in previous reports. The thermal expansion data previously available in the literature for each of those materials, over a smaller temperature range than we covered, showed wide scatter. Accordingly, there was no standard value against which to compare our results, which lay in general near the high-expansion edge of the scatter band of results.

During the redesign and construction of the hot-zone assembly for the x-ray furnace a careful check on possible errors was made. It was found that the size and alignment of the view holes through the heat shields and the vacuum-chamber wall were such that the angular aperture of the optical pyrometer was not filled with radiation from the black-body hole in the specimen. (The Pyro Micro-optical Pyrometer made by the Pyrometer Instrument Company with a 5-5.6 inch working distance has the relatively large angular aperture of about 6 degrees.) Thus, the specimen temperatures reported for given thermal expansions have been lower than the true temperatures.

The new furnace assembly, with enlarged viewing holes, has now been put into operation. The temperature of a specimen of commercial tantalum was measured simultaneously with the optical pyrometer and an inserted Pt-Rh vs. Pt thermocouple while it was heated in this new furnace assembly. The optical pyrometer was sighted into a hole (1/64 inch diameter and 1/8 inch deep) drilled in the specimen. A computed Fresnel correction, which was experimentally verified within 5°C, was applied to the fused-quartz window. A thermocouple well was also drilled in the specimen so the thermocouple was within 1/64 inch of the sighting hole. Comparative temperatures as read by the optical pyrometer and thermocouple are given in Table D-I.

Table D-I Comparison of Temperatures Measured by Thermocouple and Optical Pyrometer

	Indicated Temperature (°C)				
Thermocouple	749	853	895	1011	1293
Optical Pyrometer	733	840	890	1014	1304

The results show, within the accuracy of the techniques, that with the new arrangement the optical pyrometer gives the correct temperature. The thermal expansion work on TiC and tungsten has been redone using the new heating-zone assembly and is reported in Table D-II, along with new data obtained for ZrC. Agreement with the relatively recent x-ray data of Mauer and Bolz[1] is now good for the entire temperature range within which they made measurements.

Table D-II Thermal Expansion of TiC, ZrC, and Tungsten

TiC							
Temperature	(°C)	25	754	1016	1266	1516	1767
Expansion	(%)	.000	.547	.785	1.02	1.26	1.49
Expansion*	(%)	.000	.531	.760	1.00	-	-
ZrC							
Temperature	(°C)	25	754	1011	1267	1545	1772
Expansion	(%)	.000	.474	.666	.852	1.04	1.24
Expansion*	(%)	.000	.462	.640	.820	-	-
W							
Temperature	(°C)	25	754	1009	1273	1522	1777
Expansion	(%)	.000	.344	.475	.625	.763	.919
Expansion*	(%)	.000	.345	.476	.628	-	-

*Interpolated from the data of Mauer and Bolz.[1]

The previous discussion of the type and amplitude of the atomic vibrations is not changed, but the reported amplitudes and corresponding Debye temperatures must be recalculated. All data given in earlier reports will be recalculated and summarized in the next quarterly report.

(1) F. A. Mauer and L. H. Bolz, "Measurement of Thermal Expansion of Cermet Components by High Temperature X-ray Diffraction," NBS (Dec. 1955), ASTIA AD 95529.

The x-ray furnace has been rebuilt with the following design improvements. The hot-zone assembly now contains two plug-in units. One consisting of the specimen holders and radiation shields should facilitate periodic reconditioning, such as replacing radiation shields. The second consists of the heater supports which plug into their electrodes and have better rigidity and electrical contact than previously. Other changes are improved radiation shielding, a new shutter for the pyrometer window, and a thicker, better polished beryllium x-ray window in the furnace shell.

During the next quarter we expect to extend the measurements on TiC and ZrC to above 2000°C. A complete summary of vibrational amplitudes, thermal expansion, and Debye temperatures of TiC, ZrC, and tungsten will be prepared for the corrected temperature measurements. Studies will also begin on the effect of metal:metalloid atom ratio on the thermal expansion and vibration amplitudes of TiC and ZrC.

E. Galvanomagnetic Measurements

J. Piper

During the past quarter galvanomagnetic measurements have been made on a variety of face-centered-cubic refractory carbides of both IVa and Va Group metals. From these data further information has been obtained regarding the energy dependence of the density of valence-electron states for these materials.

1. Experimental

The Hall coefficients and electrical resistivities of a series of hot-pressed refractory carbides are presented as functions of temperature in Figures E-1 and E-2. Pertinent data regarding the samples shown in the two figures are given in Table E-I. A solid line in Figures E-1 and E-2 indicates that the effect was measured at small temperature intervals; a broken line

Table E-I Samples Used for Figures E-1 and E-2

Material	C/Me (Atomic Ratio)	Density	Major Impurities (by weight)
TiC	0.9[illegible]	0.86	-
ZrC	0.83	0.98	Free C - 1.75%, N - 1.42%
HfC	0.85	0.80	Free C - 0.52%, N - 0.80%
CbC	0.99	0.85	Free C - 0.36%
TaC	0.95	0.80	-

merely connects the experimental points that are shown. No corrections have been made for porosity of the sample. The 4.2°K points for both TaC and CbC must be regarded with some caution as the suppression of the superconductivity of the samples with a magnetic field may not have been complete. However, a magnetic field dependance of the Hall coefficient was not observed for either material, and only CbC continued to show a slight field dependance of its resistivity at 12.5 k gauss. The large relative spread in experimental points for the Hall coefficients of CbC and TaC is a result of the small magnitude ($\sim$0.1μ V) of the Hall voltage, which is limited by the small Hall coefficient, the maximum available magnetic field, and the maximum tolerable (ohmic heating) current.

2. Discussion

The most prominent features of the values presented in Figures E-1 and E-2 are the differences in magnitude and temperature dependence of the Hall coefficients between the IVa and Va carbides. In comparison, only minor

differences in properties are observed for carbides within each group. These features may be interpreted in terms of a two-band model. Calculations by Calloway[1] on the band structure of MX-type compounds, where M is a transition metal, indicate that the density of valence-electron states near the Fermi levels for these compounds is large and fluctuating. However, the large Hall coefficients R found for the IVa carbides indicate that a conduction band containing a relatively few electrons (~0.1 per metal atom) must be providing a major portion of the change transport.

If we assume that the conduction band has a standard form and provides most of the transport - as supported by the small magnetic-field dependance of the Hall coefficient and resistivity reported previously for TiC[2] - then the following analysis indicates the features of the band structure which determine the temperature dependance of R.

The Hall coefficient R is related to the concentration of charge carriers n_c by

$$R(T) \sim \frac{1}{en_c(T)} \tag{1}$$

where e is the charge of the carrier and both R and n_c are temperature dependant.

The temperature dependance of n_c is quite generally given by

$$n_c(T) = \int_0^\infty \frac{g_c(E)\,dE}{e^{(E-E_F)/kT} + 1}, \tag{2}$$

where g_c is the density of states per unit energy within the conduction band and E_F, the Fermi energy, is a function of temperature. The temperature dependance of E_F in turn is a function of the total density of states g(E) given by

$$N = \int_0^\infty \frac{g(E)\,dE}{e^{(E-E_F)/kT} + 1}, \tag{3}$$

where N is the total number of valence electrons and, therefore, independent of T.

---

1. J. Calloway. "d Bands in Cubic Lattices. III" Phys. Rev. 121, 1351 (1961).

2. Semiannual Progress Report, December 31, 1961. "Research on Physical and Chemical Principles Affecting High Temperature Materials, etc." - Contract No. DA-30-069-ORD-2787.

Solution of Equation (3) to the first non-vanishing term in T provides the relation

$$E_F(T) - E_F(0) = -\frac{\pi^2}{6} (kT)^2 \frac{g'(E_F)}{g(E_F)}, \qquad (4)$$

and the solution of Equation (2) for a standard band ($g_c \propto E^{1/2}$) and a large value of E_F/kT gives

$$\frac{n_c(T)}{n_c(0)} = \left[\frac{E_F(T)}{E_F(0)}\right]^{3/2} \qquad (5)$$

From Equations (1), (4), and (5) we obtain the expression

$$\left[\frac{R(0)}{R(T)}\right]^{2/3} = 1 - \frac{\pi^2}{6} \frac{(kT)^2}{E_F(0)} \frac{g'(E)}{g(E)}. \qquad (6)$$

While this derivation is rigorous only in the low temperature limit, the qualitative dependance of the Hall coefficient as a function of temperature upon the form of the density-of-states curve remains similar at higher temperatures.

According to Equation (6) and the data presented in Figure E-1, $g'(E)/g(E)$ is large and negative for the IVa carbides, while the same factor may be positive for the Va carbides. These features are very roughly illustrated in Figure E-3. The vertical lines marked ZrC and CbC indicate Fermi levels which are in accord with the Hall effect data for the IVth and Vth group carbides respectively.

Several comments regarding the features of Figure E-3 are pertinent.

a. The small Hall coefficients for the Va carbides suggest (from Equation (1) that there is about one electron per metal atom in the conduction band of these carbides in contrast with ~0.1 per metal atom for the IVth group carbides. In view of the increase in valence-electron concentration of 1 electron per metal atom in the step from IVth to Vth group carbides, most of the increment of valence electrons may appear to have entered the conduction band. Under these conditions the minimum in the dashed curve for g(E) would be lower and much broader than indicated in Figure E-3. The CbC Fermi level would be displaced to a higher energy. It is likely, however, that some "hole" conduction in the second band is reducing the magnitude of the Hall coefficients and thus increasing the apparent electron concentration for the Va carbides. The hole conduction, in turn, might be expected to provide a

measurable magnetoresistance. Preliminary measurements, however, indicate that the magnetoresistance is no larger than in the IVa carbides, and it remains to be seen whether hole conduction is actually important in the Va carbides.

b. In Figure E-3, the total density of states for the Va carbides is represented as smaller than that for the IVth group materials. However, there is as yet no very substantial evidence for this.

c. The shape of the density-of-states curve for the region intermediate between ZrC and CbC is open to conjecture, and its determination requires work on solid solutions of the two materials.

d. Two assumptions made in the above discussion must be considered with some reservation. The first is that of negligible conduction in a second band for the IVth group carbides; the other, that the band structure remains unchanged with the change in core potential from the IVth to the Vth group metals. Galvanomagnetic data on high-quality single crystals and on solid solutions will probably be needed before these assumptions may be critically appraised.

3. Future Work

Work toward the elucidation of resistivity differences in different samples of the same carbide has continued during the past quarter, and while there is insufficient information to support definite conclusions, there are indications that nitrogen "doping" is at least partially responsible. Further examination of the effect of partial replacement of carbon with nitrogen and boron is therefore contemplated. This, and measurements on ZrC/CbC solid solutions will provide information on the density of valence-electron states in the intermediate region. An equimolar solution of ZrC and CbC is presently being prepared. A furnace in which galvanomagnetic measurements can be made at temperatures up to 1000°C has been designed and will be constructed.

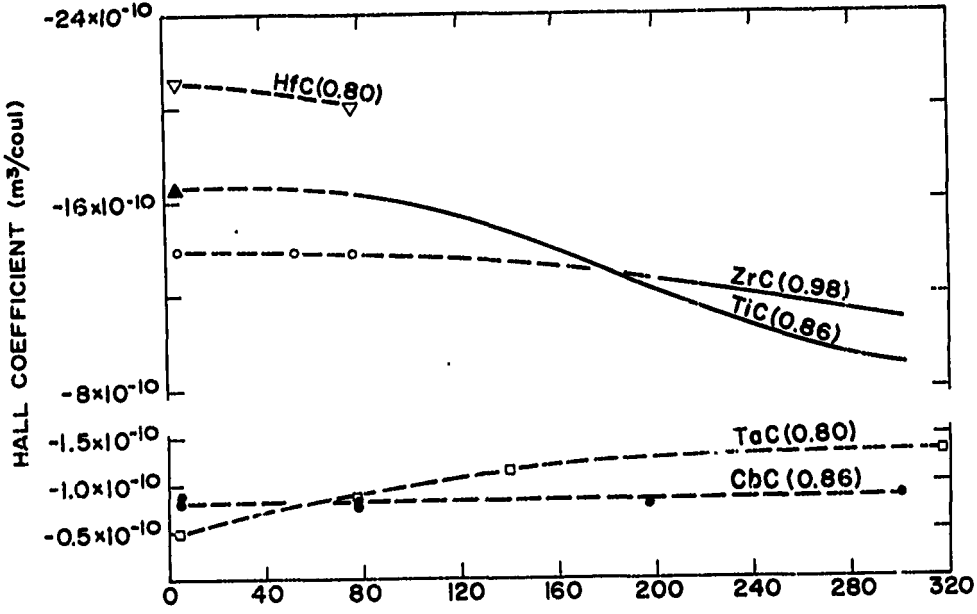

FIGURE E-1

HALL COEFFICIENT OF SOME fcc REFRACTORY CARBIDES

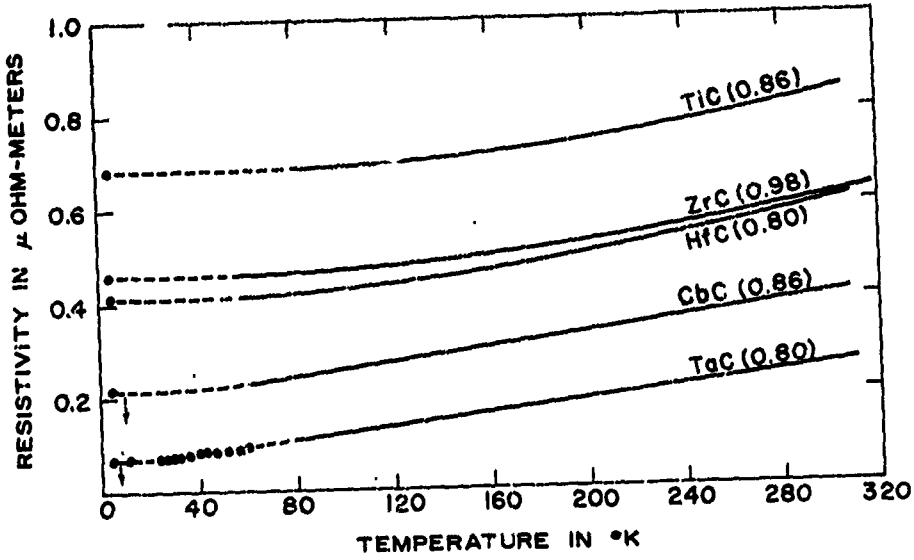

FIGURE E-2
RESISTIVITY OF SOME fcc REFRACTORY CARBIDES

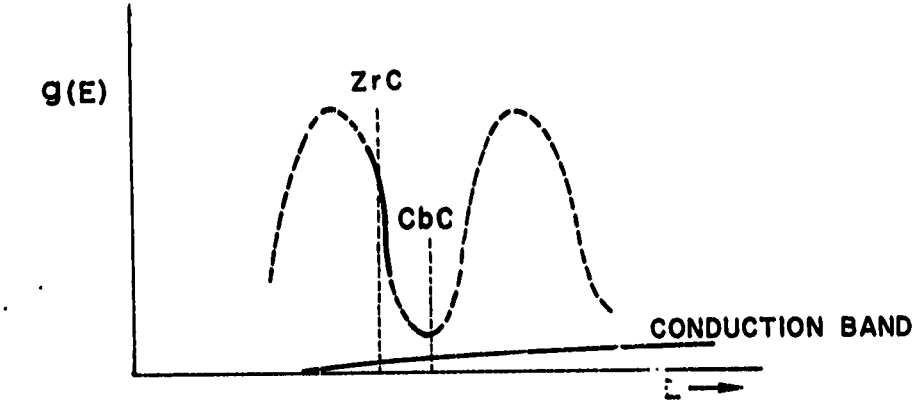

FIGURE E-3 DENSITY OF ELECTRON STATES

F. Materials Preparation — I. Binder

The production of reproducible, characterized specimens of refractory carbides and borides in a variety of shapes, as required for various measurements, is the object of this work. It is desirable that some of these specimens be of high purity so that the properties of each pure compound can be established as a basis from which to determine the influence of impurities upon properties.

Tables F-I and F-II contain the analytical results for many of the lots of refractory carbides and borides produced by us as -200 mesh powders and for which analytical results have been received. The purity of the material is shown by the total impurity content. This has been selected as a criterion rather than the content of the two major constituents because analyses for large amounts of the metals, carbon, or boron may contain errors as large as 0.5-1.0%. The total analytical uncertainty is less when the small errors in the determination of each impurity are summed. A spectrographic analysis is used to insure that no metallic impurity is overlooked.

The batches of compounds as originally prepared carry C- or B- lot numbers. These compounds were made by reacting graphite or boron powder with the appropriate powdered metal, metal hydride, or metal oxide. The reaction was carried out in an induction-heated graphite container connected by closely fitting mechanical joints to a source of purified hydrogen and to a graphite exit stack at which the hydrogen is burned. Many of these batches have been purified by heating in a vacuum of 10^{-5} - 10^{-6} mm. The resulting material is designated by a V- lot number. The vacuum treatment generally consisted of heating slowly and pausing at temperatures where gas evolution occurred until this was substantially complete. The highest temperature reached and the time held are given in the tables. The temperatures were measured with an optical pyrometer, and corrections have been added for the window and prism losses (50°C) and for an emittance of 0.4.

The borides and carbides of the Va Group metals (TaC, CbC, TaB_2, CbB_2) have been made with good to excellent purities. The results could probably still be improved by the application of vacuum purification treatments.

Considerable more difficulty has been encountered with the carbides

and borides of the IVa Group metals (TiC, TiB_2, ZrC, ZrB_2, HfC, and HfB_2). Zirconium carbide and diboride have been made in good to very good purity, but not with regularity. Titanium carbide and diboride have not yet been made to the desired standards of 99.5 + % purity, except that Lot V-18 of TiB_2 may reach this if its oxygen content, not yet reported, is < 0.2%. The hafnium compounds, made in only a few runs, have not yet reached the standard.

Vacuum purification of these carbides and borides of the Group IVa metals has been shown to be quite effective, though not a cure-all. Nitrogen can be removed from TiC, TiB_2, HfC, HfB_2, and ZrB_2 at about 2250°C. Possibly it can be removed from ZrC at higher temperatures. However, this is one element which can be largely prevented from entering the material by giving particular care to keeping the system tight and to gettering the atmosphere while forming the compound.

Oxygen and carbon contents appear to be related as one would expect. In general these materials have contained more carbon (free carbon in carbides) than oxygen. Under these conditions oxygen has been relatively easy to remove, presumably as CO, at temperatures as low as 1600°C. Whether a considerable excess of oxygen would be removed by volatilization at a practical temperature is uncertain. Mass spectrometric work here has shown that ZrO could be evaporated preferentially from ZrB_2 at 2100°C. Carbon, on the other hand, has been very difficult to remove when it is present in large amounts. In future work, attempts will be made to keep the free carbon low in the original batch. In cases where the carbon content considerably exceeds the oxygen content, several methods will be tried for adding oxygen to aid in the removal of carbon.

The metallic impurities in these carbides and borides are generally low. They are pushed even lower by vacuum heat treatments as is shown in Table F-III for some typical materials. The iron and chromium probably come mainly from the stainless-steel mortar used in crushing the partially sintered masses to fine powder.

Table F-I Analyses of Carbides (%)

Compound	Lot	C/Me [a]	Free C	N	O	Total Impurity	Vacuum Treatment
CbC	C-25	0.97	0.11	0.04	0.048	0.30	
	C-36	0.997	0.36	0.03	0.054	0.59	
TaC	C-24	0.99	0.10	0.01	0.02	0.22	
	C-40	1.00	0.10	<0.01	0.026	0.19	
	C-42A	0.975	<0.01	<0.01	0.023	0.04	
TiC	C-5	0.965	0.63	1.28	0.57	.83	
	V-34*	0.96	0.60	0.27	0.072	1.00	½ hr 2310°C
	C-37	0.965	0.98	0.62	0.1[illegible]	2.06	
	V-51*	0.945	0.52	0.70	0.04	1.36	1 hr 1770°, 5 m. 1920°C
	C-38	0.94	0.64	0.57	0.20	1.54	
	C-15	0.85	0.61	1.01	-	-	
	V-2*	0.89	0.05	0.93	-	-	Solid sample 10 m. 2130°C
	C-16R	0.845	5.24	2.48	-	-	
	V-8*	0.90	4.92	2.17	-	-	2½ hr 1710°C
	V-8R*	0.94	3.45	0.15	-	-	Above + 1½ hr 2240°C
	V-27**	0.91	6.81	1.94	-	-	1½ hr 1810°C
	V-35*	0.993	4.92	0.13	0.09	-	½ hr 2360° + ½ hr 2500°C
	C-41	0.93	2.02	0.57	0.27	3.0	
	V-65	0.97	0.94	0.40	0.023	1.40	1½ hr 2270°C
	C-22	0.96	0.50	0.82	-	-	
	V-17	-	0.28	0.60	0.06	-	10 = 2150°C
ZrC	C-20	0.95	0.41	0.27	0.47	1.32	
	V-13*	0.965	<0.05	0.28	0.065	0.37	1½ hr 2240°C
	C-21	0.95	0.37	0.35	0.32	1.14	
	C-31	0.93	0.82	0.06	0.30	1.26	
	C-43	0.869	1.23	0.19	0.37	1.83	
	V-58*	0.89	0.37	0.16	0.045	1.15	1 hr 2230°C

Table F-I (continued)

Compound	Lot	C/Me [a]	Free C	H	O	Total Impurity	Vacuum Treatment
HfC	C-17	0.85[b]	0.52	0.80	0.23	1.6	
	C-19	0.87[b]	1.55	0.59	0.08	2.22	
	V-12*	0.98[b]	1.21	0.34	0.08	1.69	1 hr 2200°C

a - Atomic ratio of combined carbon to major metal constituent.

b - The zirconium content ($2\frac{1}{2}\%$) is included as an equivalent number of moles of hafnium in calculating C/Me.

* - Produced by vacuum purification of lot immediately preceding in Table.

** - V-27 produced from part of C-16R.

Table F-II Analyses of Borides (%)

Compound	Lot	B/Me[a]	C	N	O	Total Impurity	Vacuum Treatment
CbB_2	B-48	2.00	0.21	< 0.01	0.116	0.49	
TaB_2	B-32	1.90	0.14	0.04	0.113	0.43	
	B-49	2.12	0.07	< 0.01	0.077	0.35	
TiB_2	B-20A	-	1.35	1.07	Est. 0.8	Est. 0.8	
	V-15*	2.06	0.87	0.04	0.4	1.5	10 m 2250°C
	B-21	-	0.35	0.34	-	-	
	V-18*	-	0.24	0.05	-	-	50 m 2240°C
	B-51	2.06	1.56	0.01	0.34	2.05	
	V-55*	2.13	1.27	< 0.01	0.17	1.60	4 h 1275°C
	V-57*	2.17	1.20	< 0.01	0.024	1.37	10 m 2310°C
	B-55	-	1.62	< 0.01	0.40	-	
ZrB_2	B-14	-	0.9	-	-	-	
	V-7*	-	< 0.05	-	0.24	-	1 h 1800°C
	B-19	-	0.61	1.03	-	-	
	V-25*	2.1	0.47	0.10	-	-	1/2 h 2220°C
	B-23	2.07	0.21	0.12	Est. 0.4	Est. 0.9	
	V-23*	1.85	0.05	< 0.05	0.13	0.25	1/2 h 2260°C
	B-24	1.87	0.24	0.08	Est. 0.3	Est. 1.05	
	V-24*	1.85	0.04	< 0.05	0.097	0.25	1 h 2080°C
	B-36	1.98	0.93	0.01	-	Est. 1.55	
	V-32*	2.06	0.81	0.002	0.15	1.10	1/2 h 2120°C
	B-43	2.11	1.10	0.005	0.13	1.45	
	V-44*	1.85	1.04	< 0.01	0.022	1.15	1/2 h 2290°C
HfB_2	B-15	1.96[b]	0.19	0.37	0.64	1.45	
	B-18	2.40[b]	0.60	0.41	0.095	1.50	
	V-16*	2.35[b]	0.56	0.03	0.083	0.83	1/2 h 2300°C

* - Produced by vacuum purification of lot immediately preceding in Table.

a - Atomic ratio of combined carbon to major metal constituent.

b - The zirconium content (2 1/2%) is included as an equivalent number of moles of hafnium in calculating C/Me.

Table F-III Spectrographic Analyses (%)

Material		Fe	Si	Cr	Al	V	Cu	Mn	Mg	Others
TaC	C-42A	n.d.**	n.d.	n.d.	n.d.	0.05	0.0003	n.d.	n.d.	B 0.0006 Ti 0.003 Cu .005
TaB_2	B-49	0.16	n.d.	0.038	n.d.	-	-	-	0.002	
TiC	C-37	0.10	0.02	0.03	0.02	-	-	-	-	
	V-51*	0.04	0.009	0.025	0.017	n.d.	0.006	0.001	0.0002	
	C-41	0.10	0.045	0.021	n.d.	-	-	-	-	
	V-65*	0.003	0.007	0.01	n.d.	0.006	<0.0006	0.002	n.d.	
TiB_2	B-51	0.12	0.018	-	n.d.	-	-	-	0.0006	
	B-57*	0.12	0.005	0.022	n.d.	n.d.	0.006	n.d.	0.0002	Ni 0.03
ZrC	C-43	0.039	n.d.	0.048	n.d.	0.002	0.002	0.0006	n.d.	Ti .02 B 0.001
	V-58*	n.d.	n.d.	0.048	n.d.	n.d.	n.d.	n.d.	.002- .0002	P 0.0006
ZrB_2	B-47	0.16	0.01	0.05	<0.01	-	-	-	<0.01	Ti .04 Ni<0.01
	V-44	0.05	n.d.	0.035	n.d.	0.009	n.d.	n.d.	0.0006	Ti .035 Ni n.d.

* Produced by vacuum purification of lot immediately preceding in this table.

** n.d. = not detected.

G. Mechanical Property Measurements

1. Creep of Refractory Materials

F. G. Keihn

The mechanical properties of rocket-nozzle materials are very important since nozzles are subjected to considerable loads and to high thermal stresses during operation. The strengths of materials must, of course, be known at the operating temperatures to predict their behavior under the stresses involved, but that is not enough. The ability to deform plastically and so reduce stress concentrations is also vital. It is particularly important to determine the plastic behavior of refractory carbides and borides at high temperatures, because they are notably brittle at ordinary temperatures. The high-temperature creep furnace has now been used to test a sample of tantalum in tensile creep at various temperatures in the general range 1000-1200°C, and two abortive runs have been made on TiB_2.

The deformation of tantalum was measured to within 0.01 mm by using a telemicroscope to observe fiducial marks on the sample. Figures G-1 and G-2 give the deformation vs. time for this sample under various conditions of temperature and stress. A power failure at the local utility company occurred during this test; the data in Figure G-1 being taken before, and that in Figure G-2 after this occurred. Since the beam-leveling device of the creep machine cannot back up, any specimen under test when a power failure occurs will be strained by nearly the amount of its own contraction plus that of the grips and pull-rods during the cooling to room temperature.

Dorn[1] gives the reaction-rate expression $\frac{d\epsilon}{dt} = S'e^{B\sigma} e^{-\frac{\Delta H}{RT}}$ for creep where $\frac{d\epsilon}{dt}$ is the creep rate, S' a structure-sensitive parameter, B the stress constant, σ the stress, ΔH the activation energy for creep, R the gas constant, and T the absolute temperature. The combined factor $S'e^{B\sigma}$ is termed the Zener-Hollomon parameter. Assuming this equation one may compute the activation energy if one measures the creep rates at two temperatures while keeping the stress and sample structure essentially constant. Similarly the stress constant B may be obtained from two creep rates at different stresses but constant temperature and structure.

---

1. J. E. Dorn, Creep and Recovery, p. 255-283, Am. Soc. Metals, 1957.

Murphy and Uhrig[2] measured the creep of tantalum at temperatures up to 600°C and stresses between 12 and 20 ksi. They applied Dorn's equation to their data and determined average values for ΔH and B of 109.6 kcal/mol and 5.65×10^{-4} in^2/lb respectively. Extrapolating with these values to 1025°C gives a creep rate of 1×10^{-2}/hr at 9.5 ksi compared to the 6×10^{-3} measured in this experiment. The creep rates measured after the power failure were considerably lower than would be predicted from the data of Murphy and Uhrig. This is probably a result of straining and polygonizing the sample during cooling and reheating. Both strain hardening and polygonization are known to affect strongly the creep behavior of metals. The primary purpose for working on tantalum was to try out the testing method, so no further collection of data on tantalum is planned.

Since the phase diagrams of the refractory metals with boron are not very well known, it was not possible to say whether low-melting liquids might be formed between TiB_2 and tantalum, molybdenum, or tungsten. To determine the suitability of these metals for grips, a series of experiments was made. Pieces of TiB_2 in contact with tantalum, molybdenum, or tungsten were heated in a good vacuum. These samples were continuously observed through an optical pyrometer. TiB_2 on tantalum and tungsten was heated to a brightness temperature of 2100°C with no melting. On removal from the furnace these metals showed only small discolorations at the area of contact. When TiB_2 and molybdenum were heated, however, there were indications of a liquid at 2010°C and rapid melting at 2060°C (uncorrected brightness temperature). It appears that either tantalum or tungsten grips could be used with TiB_2 up to 2100°C without serious reaction occurring.

A commercial TiB_2 tensile specimen was tested in creep at a brightness temperature of 1515°C using tantalum grips. Under a stress of 4.7 ksi the creep rate was below 1×10^{-4}/hr. A second loss of power to the building caused the fracture of this specimen at an unknown stress and temperature during its cooling. A second TiB_2 sample was lost when it was overheated (apparently through a thermocouple failure), reacted with the tantalum grips, and partially melted.

---

2. G. Murphy and R. E. Uhrig, U.C. A.E.C. Report TID-5 , August 1, 19 .

Future Work. Two more TiB_2 specimens are on hand and will be tested at temperatures above 1500°C. The measurement of temperature in these creep experiments is very important, the data of Murphy and Uhrig,[2] for example, showing that the creep rate of tantalum doubles for a 25°C temperature rise in the range near 1100°C. However, the attachment of any thermocouple to the sample is impractical and undesirable, and a black-body hole for optical measurement of temperature cannot be tolerated in a creep specimen. Accordingly, a dummy specimen containing such a hole and made of the material to be tested will be heated in the creep furnace. Temperatures will be measured both on the specimen surface and on the bottom of the hole, and later the correction thus determined will be applied to temperatures read on the surface of creep samples.

2. Mechanical Properties of Tungsten — R. L. Cummerow

Preliminary plans are under way to measure the yield stress and the steady-state creep rate as functions of temperature in the general range 1000-2500°C for tungsten crystals prepared in the "cleanest" way possible. The crystals will be prepared with an electron-beam zone-melting apparatus that will be kept completely free from carbon and other interstitial impurities by use of a Varian diffusion pump, effective oil traps for the roughing pump, and non-organic gasket materials. After the properties of the hyperpure tungsten have been established, it is planned to make the same type of measurements on tungsten single crystals that have been doped controllably with either substitutional or interstitial atoms.

The power supply for the electron-beam melting apparatus is being ordered, and work on a cathode design is under way. Preliminary design work has begun on the high-temperature tensile apparatus to be used for making the yield-stress and creep measurements.

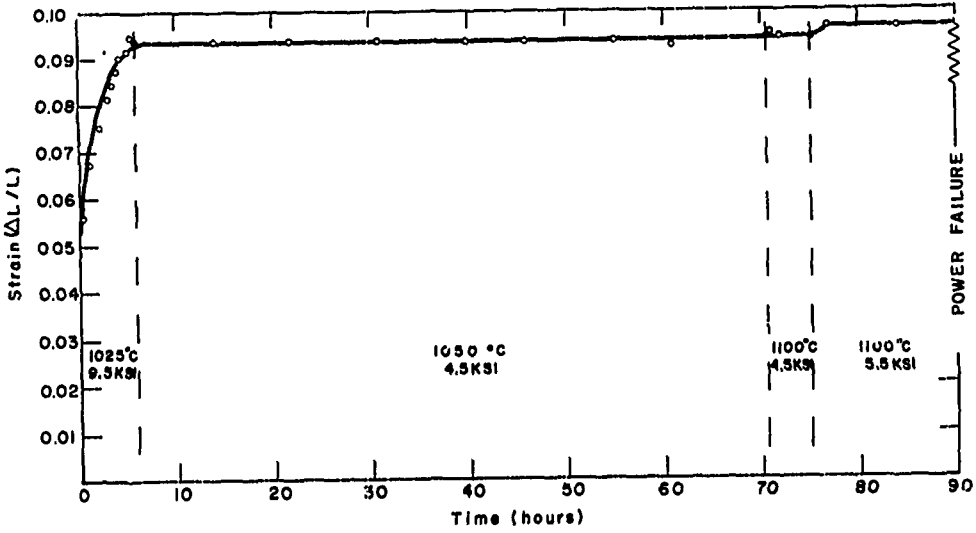

FIGURE G-1. CREEP TEST OF TANTALUM.

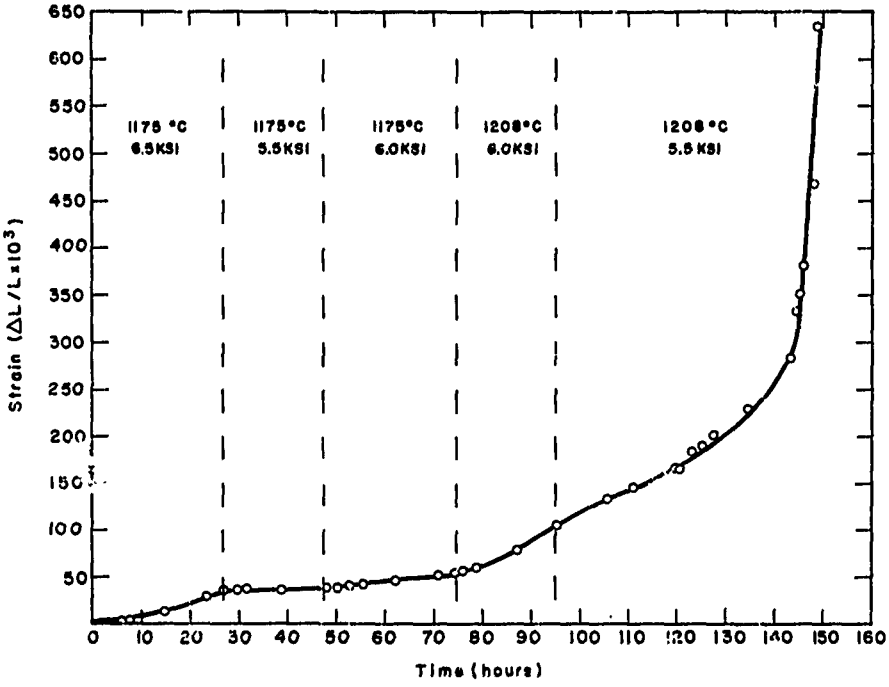

FIGURE G-2 . CONTINUATION OF CREEP TEST OF TANTALUM.

IV DISTRIBUTION

Advanced Research Projects Agency (6)
Washington 25, D. C.
Att: Advanced Propellant Chemistry Office

National Aeronautics and Space (7)
Admin.
Washington 25, D. C.
Att: Office of Technical Information and Educational Programs
Code ETL

National Bureau of Standards
Washington 25, D. C.
Att: Dr. S. Madorsky

Att: Dr. Charles W. Beckett

Oregon Metallurgical Corporation
Albany, Oregon
Att: Mr. Russell G. Hardy

U.S. Atomic Energy Commission
Office of Technical Information Extension
Oak Ridge, Tennessee

U.S. Bureau of Mines
Pittsburgh 13, Pennsylvania
Att: M. M. Dolinar, Reports Librarian, Explosives Research Lab.

Institute for Defense Analyses
Research and Eng. Support Division
Attn: Technical Information Office
1825 Connecticut Avenue, N.W.
Washington 9, D. C.

Commander
Army Ordnance Missile Command
Redstone Arsenal, Alabama
Att: Technical Library

Att: ORDXR-OR

Att: ORDXR-IXO

Att: ORDXR-RFP2

Att: ORDXR-RRH, Dr. T. A. Barr

New York Ordnance District, U. S. Army
New York 3, New York
Att: Facilities and Resources Branch

Att: ORDEH-O-TA

Office, Chief of Ordnance
Washington 25, D. C.
Att: ORDTB

Ordnance Office
Duke Station
Durham, North Carolina

Ordnance Materials Research Office
Watertown Arsenal
Watertown 72, Mass.

Dr. A. P. Levitt
Watertown Arsenal Laboratories
Watertown, Mass.

Aberdeen Proving Ground
Maryland
Att: Ballistic Research Lab.
ORDBG-BLI

Picatinny Arsenal
Dover, New Jersey
Att: Library

Diamond Ordnance Fuze Laboratories
Washington 25, D. C.
Att: ORDTL (012)

U.S. Naval Air Missile Test Center
Point Mugu, California
Att: Technical Library

(5) U.S. Naval Ordnance Laboratory
Silver Spring, Maryland
Att: Library

U.S. Naval Ordnance Test Station
China Lake, California
Att: Technical Library Branch

U.S. Naval Propellant Plant
(12) Indian Head, Maryland
Att: Technical Library

U.S. Naval Weapons Laboratory
Dahlgren, Virginia
Att: Technical Library

Office of Naval Research
Washington 25, D. C.
Att: Code 429

U.S. Naval Research Laboratory
Washington 20, D. C.
Att: Chemistry Div., Code 6130
R. R. Miller

Bureau of Naval Weapons
Washington 25, D. C.
Att: RAAP-2

Att: RAAP-4

Att: RAAP-331

Att: RLI-3 (2)

Att: RRRE-6

Special Projects Office
Department of the Navy
Washington 25, D. C.

Air Research and Development Center
Andrews AFB, Washington 25, D. C.
Att: RDRAPR

Air Force Flight Test Center
Edwards AFB, California
Att: FTR

6593rd Test Group (Dev.)
Air Force Systems Command
Edwards AFB, California
Att: DGPS

Air Proving Ground Center
Elgin Air Force Base, Florida
Att: PGAPI

Air Research and Development Command
Wright-Patterson AFB, Ohio
Att: WWRCPT-1

Air Force Systems Command (2)
Aeronautical Systems Division
Wright-Patterson AFB, Ohio
Att: Mr. W. G. Ranke
Code: ASRCNC

Headquarters, Space Systems Division
Air Force Systems Command
Los Angeles 45, California
Att: SSC

Aeronautical Systems Division
Wright-Patterson AFB, Ohio
Att: ASRCEM-1

Armed Services Tech. Info. Agency (10)
Arlington 12, Virginia
Att: TIPCR

British Defence Staff (4)
British Embassy
Washington, D. C.
Att: Scientific Information Center

Defence Research Member (4)
Canadian Joint Staff (9)
Washington 8, D. C.

Aerojet-General Corporation (3)
Sacramento, California
Att: Tech. Inf. Office

Aerojet-General Corporation
Azusa, California
Att: Library

Aeronutronic
Newport Beach, California
Att: L. H. Linder, Mgr.
Tech. Inf. Dept.

Aerospace Corporation (2)
Los Angeles 45, California
Att: Tech. Inf. Center
Acquisitions

Alpha Research and Dev., Inc. (2)
14323 So. Western Avenue
Blue Island, Illinois
Att: Dr. Robert Patrick

Allied Chemical Corporation
Research Laboratory
Morristown, New Jersey
Att: I. J. Miltrakis, Security Officer

American Cyanamid Company (2)
Stamford, Connecticut
Att: Dr. A. L. Pelker

Armour Research Foundation of
Illinois
Chicago 16, Illinois
Att: Fluid Dyn. and Prop.
Research, Dept. D

Atlantic Research Corporation
Alexandria, Virginia

Avco
Wilmington, Massachusetts
Att: Dr. E. Scalla

Att: Dr. H. L. Schick

Battelle Memorial Institute
Columbus 1, Ohio
Att: J. F. Lynch, Ceramics Div.

Att: C. S. Dumont, DMIC

Borg-Warner Corporation
Kalamazoo, Michigan
Att: J. W. Schiffel, Chief
Engineer
Special Projects Dept.

The Carborundum Company
Niagara Falls, New York

Clevite Corporation
Cleveland 8, Ohio
Att: Mr. Gail Davies

Cornell Aeronautical Laboratories
Buffalo 21, New York
Att: Mr. J. Beale

Cornell University
Materials Science Center
Ithaca, New York
Att: Prof. R. L. Sproull

DeBell and Richardson, Inc.
Hazardville, Connecticut
Att: Mr. William Eakins

The Dow Chemical Company
Midland, Michigan
Att: Dr. R. S. Karpiuk, 1710 Bldg.

E. I. duPont de Nemours and Company
Gibbstown, New Jersey
Att: Mrs. Alice R. Stewart

Esso Research and Engineering Company
Linden, New Jersey
Att: Dr. J. P. Longwell

General Electric Company
Cincinnati 15, Ohio
Att: Tech. Info. Center

Hercules Powder Company (2)
Allegany Ballistics Laboratory
Cumberland, Maryland
Att: Library

Hercules Powder Company
Rocky Hill Plant
Rocky Hill, New Jersey

Hercules Powder Company
Bacchus Works
Magna, Utah
Att: Librarian

Ionics, Inc.
1426 G. Street N.W.
Washington 5, D.C.
Att: Mr. S. G. McGriff
Asst. Director of Research

Jet Propulsion Laboratory
Pasadena 3, California
Att: I. E. Newlan, Chief
Reports Group

The Johns Hopkins University (3)
Solid Propellant Information
Agency
Applied Physics Laboratory
Silver Spring, Maryland

The Johns Hopkins University
Applied Physics Laboratory
Silver Spring, Maryland
Att: Dr. A. Westenberg

Lockheed Propulsion Company (3)
P. O. Box 111
Redlands, California
Att: Miss Belle Berlad, Librarian

Prof. J. L. Margrave
University of Wisconsin
Madison 6, Wisconsin

Minnesota Mining and Manufacturing Company (2)
St. Paul 6, Minnesota
Att: J. W. Millin

Northwestern University
Materials Research Center
Evanston, Illinois
Att: Prof. M. E. Fine

Olin Mathieson Chemical Corp. (3)
New Haven, Connecticut
Att: Miss Laura M. Kajuti

Olin Mathieson Chemical Corp.
Marion, Illinois
Att: Research Library

Rocketdyne (3)
Canoga Park, California
Att: Library 596-306

Rocketdyne
McGregor, Texas
Att: Library

Rocket Power
Pasadena, California
Att: Dr. Milton Farber, Vice Pres.

Shell Development Company
Emeryville 6, California

Space Technology Laboratory, Inc.
Los Angeles 45, California
Att: Mr. Robert C. Anderson

Thiokol Chemical Corporation
Huntsville, Alabama
Att: Technical Director

Thiokol Chemical Corporation
Elkton, Maryland
Att: Librarian

Thiokol Chemical Corporation (2)
Brigham City, Utah
Att: Library Section

Thiokol Chemical Corporation
Rocketo Operation Center
Ogden, Utah
Att: Librarian

United Technology Department
Sunnyvale, California
Att: Librarian

University of Pennsylvania
Laboratory for Research on Structure of Matter
Philadelphia 4, Pennsylvania
Att: Prof. J. N. Hobstetter

Wright Aeronautical Corporation (2)
Wood-Ridge, New Jersey

UNION CARBIDE CORPORATION:

Dr. J. C. Bowman
Mr. E. J. Boyle
Dr. R. G. Breckenridge
Dr. R. M. Bushong
Dr. R. L. Cummerow
Mr. H. A. Downey
Dr. D. M. Gillies
Mr. D. E. Hamby
Dr. A. B. Kinzel
Dr. R. A. Charpie
Helen F. Kuhns, Librar -,
Haynes Stellite Company
Dr. R. W. McNamee
Mr. R. M. Milton
Dr. John Pike
Dr. P. O. Schissel
Dr. Milton Stern
Mr. W. A. Steiner
Dr. Roy C. Sundeen
Mr. J. D. Venables
Mr. G. H. Wag :1
Mr. H. L. Willard